Inelastic electron-electron scattering for surface states on Cu(110) and Ag(110)

S. S. Tsirkin,[1] S. V. Eremeev,[1,2] and E. V. Chulkov[3,4]

[1]*Tomsk State University, Prospekt Lenina 36, 634050 Tomsk, Russia*

[2]*Institute of Strength Physics and Materials Science, Prospekt Academicheskii 2/4, 634021 Tomsk, Russia*

[3]*Donostia International Physics Center (DIPC), 20018 San Sebastián/Donostia, Basque Country, Spain*

[4]*Departamento de Física de Materiales and Centro de Física de Materiales (CFM)–Materials Physics Center (MPC), E-20018 San Sebastian/Donostia, Spain, Facultad de Ciencias Químicas, UPV/EHU, Apartado 1072, E-20080 San Sebastián/Donostia, Basque Country, Spain*

(Received 2 April 2011; revised manuscript received 21 June 2011; published 26 September 2011)

Many-body electron-electron scattering contribution to the decay rate of electron and hole excitations on the (110) surface of copper and silver is calculated within GW approximation for electron self-energy. The band structure is described using a two-dimensional model pseudopotential, which precisely reproduces the surface electronic structure at the $\overline{\mathrm{Y}}$ point. Combined with the previously calculated electron-phonon contribution, our result for the occupied state on Cu(110) agrees well with the available photoemission data.

DOI: 10.1103/PhysRevB.84.115451 PACS number(s): 68.47.De, 73.20.−r

I. INTRODUCTION

In recent years many theoretical and experimental studies were focused on electron dynamics in bulk electronic states,[1–6] surface and image potential states on clean metal surfaces,[7–15] as well as in excited states in overlayers,[16–20] adatoms,[21–25] nanoislands,[26] and nanopyramids.[27] These investigations were stimulated by the important role of electronic excitations in various physical and chemical phenomena, such as desorption process,[28] catalytic reactions,[29,30] epitaxial growth,[31] and many others. Significant progress has been achieved in the understanding of different mechanisms of the decay of the electronic excitations.[32,33]

Information on the quasiparticle lifetime τ can be derived from photoemission measurements of the linewidth of the electron state.[32] The linewidth Γ of such a state is a sum of contributions of three different processes: inelastic electron-electron scattering ($\Gamma_{e\text{-}e}$), electron-phonon interaction ($\Gamma_{e\text{-}ph}$), and electron-defect scattering ($\Gamma_{e\text{-}d}$). $\Gamma_{e\text{-}e}$ is temperature independent, while thermal broadening of the linewidth is determined by electron-phonon interaction[34,35] and scattering on thermally activated defects.[36,37]

Most theoretical and experimental investigations of the dynamics of surface excitations have been carried out for close-packed surfaces[13,14,32,33,35] and only few studies have been concentrated on open surfaces.[38–41] Open surfaces, such as fcc metal (110) surface or stepped surfaces, are of great interest, in particular, due to their high catalytic activity.[42] *Ab initio* computations of lifetimes of excited electrons (holes) in surface states are time consuming[32,33,38] and therefore the use of simplified models can be efficient in the description of the excited electron decay mechanisms. Such a model has been proposed in Ref. 43 for close-packed surfaces. Within this model the band structure of a surface is described using a pseudopotential, varying only in the direction, perpendicular to the surface, while the potential and electron density are assumed to be constant in the plane parallel to the surface. This model proved to give $\Gamma_{e\text{-}e}$ and $\Gamma_{e\text{-}ph}$ in agreement with experimental results for surface states[32,33] as well as for image-potential states[32,33] in the vicinity of the $\overline{\Gamma}$ point.

The (110) surfaces of fcc metals have a more complicated electronic structure than the close-packed surfaces. Two surface states are present in the $\overline{\mathrm{Y}}$ gap on Cu(110) (see Fig. 1) and Ag(110): the occupied one with energy of -510 meV[39] (Cu) and -0.106 meV[44] (Ag) and the unoccupied one located at 1.7 eV[45] (Cu) and 1.6 eV[46] (Ag) [energies are given relative to the Fermi energy (E_F)]. The occupied surface state (SS_{occ}) is localized in the outermost atomic layer between the atomic chains in the $(1\bar{1}0)$ direction, while the unoccupied one (SS_{unocc}) is mainly localized above the outermost atomic layer. To illustrate the spatial distribution of the surface states we show in Fig. 2 charge density distribution of SS_{occ} (a) and SS_{unocc} (b) on Ag(110), calculated using density-functional theory (DFT). It should be noted that the presence of two surface states localized in one gap with distinct spatial distribution, cannot be described within a one-dimensional (1D) pseudopotential model,[43] because only one surface state, uniformly distributed in the surface plane, can be achieved in the 1D model.

In order to study electron and hole dynamics in surface states on (110) surfaces of fcc metals, a model has been elaborated in Refs. 47 and 48. This model describes the electronic structure of (110) surfaces of noble metals by using a two-dimensional (2D) pseudopotential, varying in directions [110] (perpendicular to the surface) and [001] (parallel to the surface). The parameters of the pseudopotential are chosen to precisely reproduce the experimentally observed (or calculated from first principles, when experimental data are not available) energies of both surface states, the gap edges, and the first image potential state *at the* $\overline{\mathrm{Y}}$ *point*. The model has been used for calculations of electron-phonon coupling strength on (110) surfaces of noble metals[49,50] and proved to give values of electron-phonon coupling constant in close agreement with the experiment.[39]

In this paper we focus on electron-electron scattering. Inelastic electron-electron scattering is more sensitive to the accuracy of the description of the phase space of final states than the quasielastic electron-phonon scattering. As far as the dispersion of electronic states calculated within this model has some deviations from that calculated by means of DFT

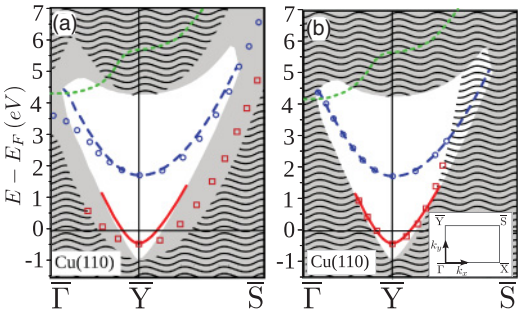

FIG. 1. (Color online) *Real band structure* of the Cu(110) surface in comparison with that obtained in the original (a) and modified (b) pseudopotential models. The *real* and model-derived projection of bulk states onto the surface Brillouin zone are represented by the gray and wave striped areas, respectively. Solid (dashed) lines denote the *real* occupied (unoccupied) surface states; squares (circles) describe the model-derived occupied (unoccupied) surface states. The green dotted line denotes the model-calculated first image-potential state. The 2D Brillouin zone is shown in the inset.

or observed experimentally, we modify the pseudopotential model[47,48] to fit the dispersion of electronic states in order to describe the phase space more accurately. We calculate electron-electron contributions $\Gamma_{e\text{-}e}$ to linewidths of excited electrons and holes in the surface states of copper and silver within the *GW* approximation, using the band structure, obtained in the modified pseudopotential model. Calculations within the original model are also performed for comparison.

The coordinate system we use is formed by the z axis along the [110] direction (perpendicular to the surface) and the y and x axes along the [001] and [1$\bar{1}$0] directions, respectively [see Fig. 2(a)]. The origin $y = 0$ is taken at the position of an atom in the outermost atomic layer. Unless otherwise mentioned, $z = 0$ corresponds to the center of the slab. In all equations atomic units are used; that is, $e^2 = \hbar = m_e = 1$.

II. METHOD

A. Modifying the 2D potential

The aim of this section is to build a simplified model that accurately describes the energies of the two surface states and the edges of the local gap over the Brillouin zone (BZ) of real metal surfaces. First we have to define what we shall

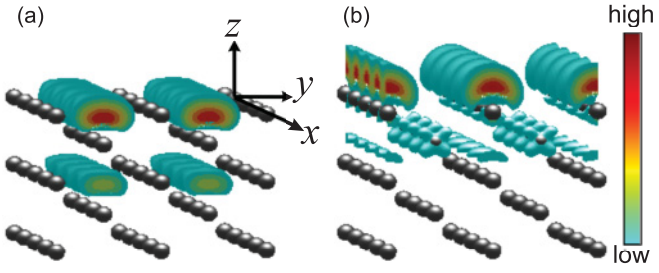

FIG. 2. (Color online) *Ab initio* (DFT) calculated charge density distribution of the occupied (a) and unoccupied (b) surface states on Ag(110). Gray balls denote the positions of Ag ions. The coordinate axes x, y, and z are chosen along the [1$\bar{1}$0], [001], and [110] directions, respectively.

treat as a "real band structure." The problem is that neither experimental measurements nor theoretical calculations give complete information on electronic structure. Experimental data are usually limited to high-symmetry points and/or small vicinities around them. Information on the dispersion of electronic states over the entire BZ can be achieved by means of DFT calculations, which are known to give an accurate description of the ground state, but they normally underestimate the energies of unoccupied states. Thus, to obtain a maximally complete picture of the band structure we make a combination of experimental and theoretical results.

First we perform DFT calculations of the surface band structure of Cu and Ag (110) using the VASP code.[51,52] In this plane-wave basis set code the interaction between ionic cores and valence electrons is described by the projector-augmented wave (PAW) method.[53,54] Generalized gradient approximation[55] is employed to evaluate the exchange-correlation energy. The 33-layer relaxed slabs are used to calculate the surface band structure for the considered materials. The calculated position of the lower gap edge and the occupied surface state at the $\bar{Y}$ point as well as their dispersion in the vicinity of $\bar{Y}$ are in a good agreement with available experimental data.[39,44] However, the energies of unoccupied surface states are underestimated, yielding 1.5 eV (Cu) and 1.4 eV (Ag), compared to the experimental results 1.7 eV[45] (Cu) and 1.6eV[46] (Ag). Therefore, we shift the dispersion curves of these states upward to reproduce the experimental values at the $\bar{Y}$ point. Unfortunately, no experimental value of the upper gap edge is available; thus, we leave its dispersion curve at the *ab initio* value of 4.25 eV (Cu) and 4.0 eV (Ag) at the $\bar{Y}$ point. This combination of experimental results and DFT calculations are later referred to as *the real band structure*.

As an example we show in Fig. 1 the surface electronic structure of Cu(110). The Ag(110) surface band structure is qualitatively similar to the Cu(110) one and it is not shown here.

Now we turn to constructing a model which accurately reproduces the *real* energy spectrum of the surfaces under consideration.

A good basis for such a model is the 2D pseudopotential, introduced in Refs. 47 and 48. Within this model calculations of electronic structure are performed using repeated slabs separated by vacuum spacings, with a period T in the direction perpendicular to the surface. In such a model one-electron wave functions and energies are obtained in the following form:

$$\Psi_{n\mathbf{k}}(\mathbf{r}) = \frac{1}{L} e^{i(k_x x + k_y y)} u_{n,k_y}(y,z), \tag{1}$$

$$E_{n\mathbf{k}} = E_{nk_y} + \frac{k_x^2}{2m_n^*}. \tag{2}$$

Here and after $\mathbf{r} = (x,y,z)$ denotes a 3D vector, L is a normalization length. The 2D wave vector $\mathbf{k} = (k_x,k_y)$ has the k_y component in the surface BZ ($-\frac{\pi}{a} < k_y < \frac{\pi}{a}$, where a is the lattice parameter), the k_x component being arbitrary. Bloch functions $u_{n,k_y}(y,z)$ obey the following normalization conditions:

$$\frac{1}{a}\int_{-a/2}^{a/2} dy \int_{-T/2}^{T/2} dz \quad |u_{n,k_y}(y,z)|^2 = 1. \tag{3}$$

In the slab model wave functions are either even (+) or odd (−) with respect to the z-mirror plane situated in the slab center, and hence they can be written as the Fourier expansion

$$u^{\pm}_{n,k_y}(y,z) = \sum_{g_y,g_z} C^{\pm}_{n,k_y,g_y,g_z} f^{\pm}_{g_y,g_z}(y,z) \tag{4}$$

in terms of basis functions $f^{\pm}_{g_y,g_z}(y,z)$:

$$f^{+}_{g_y,g_z}(y,z) = \sqrt{\frac{\delta_{g_z}}{aT}}\, e^{ig_y y} \cos(g_z z), \tag{5}$$

$$f^{-}_{g_y,g_z}(y,z) = \sqrt{\frac{2}{aT}}\, e^{ig_y y} \sin(g_z z), \tag{6}$$

where $g_y = \frac{2\pi}{a} n_y$, $g_z = \frac{2\pi}{T} n_z$ (n_y,n_z are integer), and

$$\delta_{g_z} = \begin{cases} 1, & \text{if} \quad g_z = 0, \\ 2, & \text{if} \quad g_z \neq 0. \end{cases}$$

The band structure evaluated in this pseudopotential model is shown in Fig. 1(a). As far as the parameters of the model were chosen to reproduce the energies of the two surface states, the gap edges, and the first image-potential state at the $\overline{\text{Y}}$ point, the energy spectrum obtained in the model precisely coincides with the *real* one at this point. As was shown in Ref. 48, the model-derived charge density distributions of the surface states are in good agreement with the DFT-calculated ones, represented in Fig. 2. However, as we move away from the $\overline{\text{Y}}$ point, the spectrum obtained from the 2D model deviates from the real one. For example, the width of the local energy gap becomes overestimated in the model and thus the gap survives at the $\overline{\Gamma}$ and $\overline{\text{S}}$ points of the surface BZ, while it should exist only around the $\overline{\text{Y}}$ point. The model adequately describes the dispersion of the unoccupied surface states in the vicinity of the $\overline{\text{Y}}$ point [the calculated effective mass of SS_{unocc} on Cu(110) in the $\overline{\text{Y}\Gamma}$ direction, found to be $m^* = 0.94$, is in agreement with the experimental value $m^* = 0.8 \pm 0.2$ (Ref. 56)], but the effective mass of the occupied state in the k_y direction is overestimated, yielding $m^* = 0.85$, which is significantly higher than the photoemission spectroscopy result $m^* = 0.26$[39] as well as our *ab initio* value $m^* = 0.24$. Moreover, as far as our potential does not depend on the x coordinate (direction $[1\bar{1}0]$), the effective masses m^* in the $\overline{\text{YS}}$ direction are equal to free-electron masses. Below we refer to the original 2D pseudopotential model,[47,48] described above, as *model O*.

Discrepancies between the real band structure and that calculated within the model O may result in inaccuracies in predicted lifetimes of excitations because of insufficiently accurate description of the phase space available for transitions. To overcome this problem we derive a modified 2D-pseudopotential model, which is denoted as *model M*. The modification is performed as follows.

To correctly describe the dispersion of surface states and gap edges in the $\overline{\Gamma\text{Y}}$ direction, we make our pseudopotential k_y dependent: At each k_y point of interest we fit the parameters to reproduce the key features (energies of gap edges and surface states) of the *real band structure* at this point. Figure 3 shows that the decrease of the energy gap requires the reduction of the amplitude of the pseudopotential for k_y points away from $\overline{\text{Y}}$. The band structure obtained in the model M is shown in Fig. 1(b). One can see that model M precisely reproduces the DFT-derived dispersion of the surface states and the gap edges in the $\overline{\text{Y}\Gamma}$ direction.

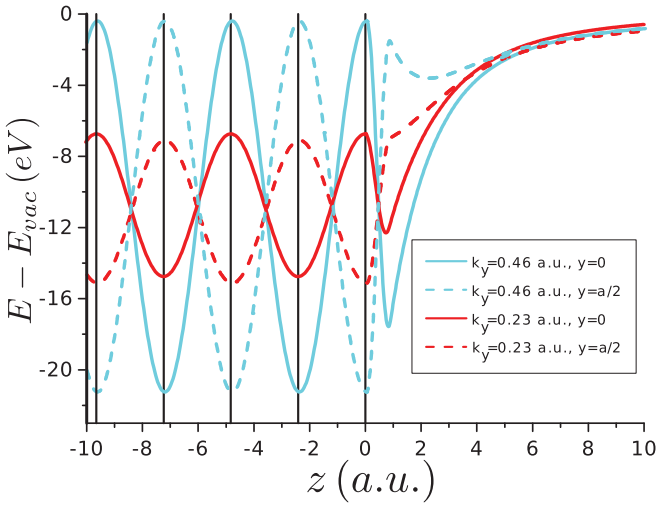

FIG. 3. (Color online) Model pseudopotential for Cu(110) at the $\overline{\text{Y}}$ point ($k_y = 0.46$ a.u.) and at the middle of the $\overline{\text{YT}}$ direction ($k_y = 0.23$ a.u.). Vertical lines indicate the positions of atomic layers. The origin $z = 0$ corresponds to the outermost atomic layer.

To fit the dispersion in the $[1\bar{1}0]$ direction (k_x component of the wave vector) to the *real band structure* we set the effective masses $m^*_n \neq 1$ [Eq. (2)]. The values m^*_n are chosen in the following way.

First we determine the effective masses of the surface states and two edges of the gap (see Table I). The dispersion of the unoccupied surface state and the upper edge of the gap show parabolic dependence on the momentum along the entire $\overline{\text{YS}}$ direction, and therefore they are accurately approximated by effective masses. However, this is not the case for the occupied surface state and the lower edge of the gap, since their dispersion deviates significantly from the parabolic law for energies above E_F. However, in the energy region $[E_{\text{occ}}, E_{\text{unocc}}]$, where the final states for electron (hole) decay are situated, we can satisfactorily fit the dispersion curves of the SS_{occ} and the lower gap edge by parabolas with effective masses m^*_{occ} and m^*_{lower}, respectively.

Finally, we need to determine m^*_n for bulk electronic states above and below the energy gap. The effective masses of the bulk electronic states above the gap are taken equal to m^*_{upper}, while masses of bulk states below the gap change smoothly from m^*_{lower} at the gap edge to m^*_0 for the lowest band obtained in the model. The value of m^*_0 is chosen to fit *ab initio* data and is equal to $m^*_0 = 1.5$ for both Ag and Cu.

TABLE I. Effective masses (in atomic units) of the lower (m^*_{lower}) and the upper (m^*_{upper}) edges of the gap and of the occupied (m^*_{occ}) and the unoccupied (m^*_{unocc}) surface states in the $\overline{\text{YS}}$ direction used in the model M.

	m^*_{lower}	m^*_{upper}	m^*_{occ}	m^*_{unocc}
Cu(110)	0.42	2.3	0.33	0.95
Ag(110)	0.34	2.4	0.37	0.90

One can see from Fig. 1(b) that the modified model describes the phase space of final states for electron (hole) decay much better than the model O does. Notable discrepancies between model M and real band structure in the $\overline{\text{YS}}$ direction are observed at energies higher than 2 eV, but this does not affect the phase space. Thus, we expect the model M to give more reliable results than the model O does.

B. Implementation of the GW method in the 2D-pseudopotential model

Within many-body theory the inelastic electron-electron scattering contribution to the linewidth $\Gamma = \tau^{-1}$ of an electron state in band i with wave function Ψ_0, energy E_0, and wave vector $\mathbf{k}_0$ is evaluated as the projection of the imaginary part of the self-energy operator Σ onto the state

$$\Gamma^{e\text{-}e}_{i,\mathbf{k}_0} = -2 \iint [\Psi_0^*(\mathbf{r}) \mathrm{Im}\Sigma(\mathbf{r},\mathbf{r}';E_0)\Psi_0(\mathbf{r}')] d\mathbf{r}\, d\mathbf{r}'. \quad (7)$$

In the GW approach[57] only the first term in the series expansion of the self-energy Σ in terms of the screened Coulomb interaction W is retained, yielding

$$\mathrm{Im}\Sigma(\mathbf{r},\mathbf{r}',E_0) = \sum_{n,\mathbf{k}}^{E_{n\mathbf{k}}\in[E_0,E_F]} \Psi^*_{n\mathbf{k}}(\mathbf{r}') \mathrm{Im}W(\mathbf{r},\mathbf{r}',|E_0 - E_{n\mathbf{k}}|)\Psi_{n\mathbf{k}}(\mathbf{r}), \quad (8)$$

where summation is carried out over all final electronic states $(n\mathbf{k})$ with energies $E_F < E_{n\mathbf{k}} < E_0$ for the electron decay or $E_F > E_{n\mathbf{k}} > E_0$ for the hole decay. The screened interaction W is given in linear response theory by

$$W(\mathbf{r},\mathbf{r}';\omega) = V(\mathbf{r}-\mathbf{r}') + \iint [V(\mathbf{r}-\mathbf{r}_1) \times \chi(\mathbf{r}_1,\mathbf{r}_2;\omega) V(\mathbf{r}_2-\mathbf{r}')] d\mathbf{r}_1 d\mathbf{r}_2, \quad (9)$$

where $V(\mathbf{r}-\mathbf{r}')$ is the bare Coulomb interaction and $\chi(\mathbf{r}_1,\mathbf{r}_2;\omega)$ is the linear density-density response function, which is evaluated from the Dyson-like equation

$$\chi(\mathbf{r}_1,\mathbf{r}_2;\omega) = \chi^0(\mathbf{r}_1,\mathbf{r}_2;\omega) + \iint [\chi^0(\mathbf{r}_1,\mathbf{r}_3;\omega) \times V(\mathbf{r}_3-\mathbf{r}_4)\chi(\mathbf{r}_4,\mathbf{r}_2;\omega)] d\mathbf{r}_3 d\mathbf{r}_4. \quad (10)$$

Here $\chi^0(\mathbf{r}_1,\mathbf{r}_2;\omega)$ is the density-density response function of a noninteracting electron system:

$$\chi^0(\mathbf{r}_1,\mathbf{r}_2;\omega) = 2\sum_{\alpha,\mathbf{k}_\alpha}\sum_{\beta,\mathbf{k}_\beta} \frac{\theta(E_F - E_{\alpha\mathbf{k}_\alpha}) - \theta(E_F - E_{\beta\mathbf{k}_\beta})}{E_{\alpha\mathbf{k}_\alpha} - E_{\beta\mathbf{k}_\beta} + \omega + i\eta} \times \Psi_{\alpha\mathbf{k}_\alpha}(\mathbf{r}_1)\Psi^*_{\beta\mathbf{k}_\beta}(\mathbf{r}_1)\Psi_{\beta\mathbf{k}_\beta}(\mathbf{r}_2)\Psi^*_{\alpha\mathbf{k}_\alpha}(\mathbf{r}_2). \quad (11)$$

In this equation α and β indicate the band numbers, $\mathbf{k}_\alpha$ and $\mathbf{k}_\beta$ are wave vectors, and η is an infinitesimally small positive constant.

Equations (7)–(10) contain integrations over the entire 3D space. The aim of this section is to simplify the calculations by reducing the dimensions and limits of integrations. This can be done by exploiting symmetry properties of the model. It is easy to show that functions $\chi^0(\mathbf{r},\mathbf{r}';\omega)$, $\chi(\mathbf{r},\mathbf{r}';\omega)$, and $W(\mathbf{r},\mathbf{r}';\omega)$ retain the symmetry of the potential; that is, they are invariant under translations like

$$\{(x,y,z),(x',y',z')\} \to \{(x+dx,y+na,z)(x'+dx,y'+na,z')\}, \quad (12)$$

where dx is arbitrary and n is integer. We introduce the transformation (denoted by tilde) of a function $A(\mathbf{r},\mathbf{r}')$ dependent on two 3D variables:

$$\tilde{A}_{\mathbf{q}}(y,z;y',z') = a\int dx e^{iq_x x} \sum_n e^{iq_y(y-y'-na)} A(0,y,z;x,y'+na,z'), \quad (13)$$

where $\mathbf{q} = (q_x,q_y)$ is an arbitrary 2D wave vector. If a function A is invariant under translation (12), the function $\tilde{A}_{\mathbf{q}}(y,z;y',z')$ depends only on 2D variables and is periodic in y and y' with a period of the lattice parameter a. Now we can rewrite Eqs. (7)–(11) in terms of the transformed functions $\tilde{W}$, $\tilde{\chi}$, and $\tilde{\chi}^0$. It follows from Eqs. (7) and (8) that the linewidth is expressed by

$$\Gamma^{e\text{-}e}_{i,\mathbf{k}_0} = -\frac{2}{a^2(2\pi)^2}\int_{-\infty}^{+\infty} dk_x \int_{-\pi/a}^{\pi/a} dk_y \sum_n^{E_{n\mathbf{k}}\in[E_0,E_F]} \iint_{-a/2}^{a/2} dy dy' \times \iint_{-T/2}^{T/2} dz dz'\ \Phi_{ik_{y0},nk_y}(y,z)\,\Phi^*_{ik_{y0},nk_y}(y',z') \times \mathrm{Im}\tilde{W}_{\mathbf{k}-\mathbf{k}_0}(y,z;y',z';|E_0-E_{n\mathbf{k}}|), \quad (14)$$

where $\Phi_{ik_{y0},nk_y}(y,z) = u_{ik_{y0}}(y,z)u^*_{nk_y}(y,z)$. Here $E_{n\mathbf{k}}$ is given by Eq. (2) with non-free-electron effective masses. The imaginary part of the screened interaction $\tilde{W}_{\mathbf{q}}$ is given by

$$\mathrm{Im}\tilde{W}_{\mathbf{q}}(y,z;y',z';\omega) = \frac{1}{a^2}\sum\nolimits_{g_{y1},g_{y2}} e^{i(g_{y1}y-g_{y2}y')} \iint_{-T/2}^{T/2} dz_1 dz_2 \times V(q_x,q_y+g_{y1};z-z_1)V(q_x,q_y+g_{y2};z'-z_2) \times \iint_{-a/2}^{a/2} dy_1 dy_2 \mathrm{Im}\tilde{\chi}_{\mathbf{q}}(y_1,z_1;y_2,z_2;\omega) e^{-i(g_{y1}y_1-g_{y2}y_2)}. \quad (15)$$

Here $V(k_x,k_y;z-z_1)$ is the 2D Fourier transform of the bare Coulomb potential:

$$V(k_x,k_y;z-z_1) = \frac{2\pi}{\sqrt{k_x^2+k_y^2}} e^{-|z-z_1|\sqrt{k_x^2+k_y^2}}, \quad (16)$$

and $g_{yi} = \frac{2\pi}{a}n_i$, where $i = 1,2$ and n_i is integer. The Dyson-like Eq. (10) is reduced to

$$\tilde{\chi}_{\mathbf{q}}(y_1,z_1;y_2,z_2;\omega) = \tilde{\chi}^0_{\mathbf{q}}(y_1,z_1;y_2,z_2;\omega) + \frac{1}{a^2}\sum_{g_{y1}} \iint_{-a/2}^{a/2} dy_3 dy_4 \times \iint_{-T/2}^{T/2} dz_3 dz_4\ \tilde{\chi}^0_{\mathbf{q}}(y_1,z_1;y_3,z_3;\omega)V(q_x,q_y+g_{y1};z_3-z_4) \times e^{i(y_3-y_4)g_{y1}}\tilde{\chi}_{\mathbf{q}}(y_4,z_4;y_2,z_2;\omega). \quad (17)$$

To calculate the response function of the noninteracting electron gas $\tilde{\chi}^0_{\mathbf{q}}(y_1,z_1;y_2,z_2;\omega)$ in terms of wave functions

(1) derived from our 2D pseudopotential model, we transform Eq. (11) via Eq. (13), replace summations over wave vectors $\mathbf{k}_\alpha$, $\mathbf{k}_\beta$ by integrations, and perform integrations over x components of the wave vectors analytically, using the quadratic dispersion in the k_x direction (2), leaving the integral over k_y for numerical computation:

$$\tilde{\chi}^0_{\mathbf{q}}(y_1,z_1;y_2,z_2;\omega) = 2\int_{-\pi/a}^{\pi/a}\frac{dk_y}{2\pi}\sum_{n_1}^{E_{n_1,k_y}<E_F}\sum_{n_2}^{\infty}\left(h^+_{n_1,k_y;n_2,k_y+q_y}(\mathbf{q},\omega) + h^-_{n_1,k_y;n_2,k_y+q_y}(\mathbf{q},\omega)\right)\Phi_{n_1,k_y;n_2,k_y+q_y}(y_1,z_1)\Phi^*_{n_1,k_y;n_2,k_y+q_y}(y_2,z_2), \tag{18}$$

where $h^\pm_{n_1,k_y;n_2,k_y+q_y}(\mathbf{q},\omega)$ is

$$h^\pm_{n_1,k_y;n_2,k_y+q_y}(\mathbf{q},\omega) = \frac{m^*_{n_2}}{2\pi}I\Bigg(-\frac{m^*_{n_2}-m^*_{n_1}}{m^*_{n_1}}Q^F_{n_1k_y}+q_x, \frac{m^*_{n_2}-m^*_{n_1}}{m^*_{n_1}}Q^F_{n_1k_y}+q_x, -\frac{m^*_{n_2}}{m^*_{n_1}}q_x^2+2\frac{m^*_{n_2}-m^*_{n_1}}{m^*_{n_1}}m^*_{n_2} \times\left(E_{n_1,k_y}-E_{n_2,k_y+q_y}\pm\omega\right)\pm\operatorname{sgn}\left(m^*_{n_2}-m^*_{n_1}\right)\Bigg). \tag{19}$$

Here $Q^F_{n_1k_y}=\sqrt{2m^*_{n_1}(E_F-E_{n_1,k_y})}$, $m^*_{n_i}$ are effective masses of energy bands in the k_x direction, which have been chosen according to the procedure described in Sec. II A. We use the notation I for integral, solved analytically

$$I(\alpha,\beta,B,\pm) = \lim_{\eta\to 0+0}\int_\alpha^\beta\frac{dx}{x^2+B\pm i\eta} = \begin{cases}\left[\arctan\left(\frac{\beta}{\sqrt{B}}\right)-\arctan\left(\frac{\alpha}{\sqrt{B}}\right)\right]/\sqrt{B}, & \text{if} \quad B>0;\\ \frac{1}{2\sqrt{|B|}}\left[\ln\left|\frac{(\beta-\sqrt{|B|})(\alpha+\sqrt{|B|})}{(\beta+\sqrt{|B|})(\alpha-\sqrt{|B|})}\right|\mp i\pi(\Theta(\alpha,\beta,\sqrt{|B|})+\Theta(\alpha,\beta,-\sqrt{|B|}))\right], & \text{if} \quad B<0.\end{cases} \tag{20}$$

Here

$$\Theta(\alpha,\beta,\gamma) = \begin{cases}1, & \text{if} \quad \alpha<\gamma<\beta;\\ -1, & \text{if} \quad \alpha>\gamma>\beta;\\ 0, & \text{otherwise.}\end{cases} \tag{21}$$

C. Details of numerical computations

Calculations are performed in the model of repeated slabs with thicknesses of 51 atomic monolayers (MLs) separated by vacuum intervals of 40 interlayer spacings $a_s = a/\sqrt{8}$. In this geometry two surfaces of the slab are present and therefore we have two surface states of each type (SS_{occ} or SS_{unocc}): an odd one and an even one. The slab thickness of 51 ML prevents interaction between these surface states. Another feature of slab geometry is that the projection of bulk states onto the surface BZ is represented by discrete bands. In the 51-layer film the average distance between levels at $\overline{\text{Y}}$ is ∼0.07 eV, which is several times less then the distance from the gap edge to the occupied surface state. Thus, we expect that the characteristics of the surface states calculated in this model will be close to that of a semi-infinite crystal.

To deal with Eqs. (14)–(18) we expand functions $\tilde{\chi}^0_{\mathbf{q}}(y_1,z_1;y_2,z_2;\omega)$, $\tilde{\chi}_{\mathbf{q}}(y_1,z_1;y_2,z_2;\omega)$, $\tilde{W}_{\mathbf{q}}(y,z;y',z';\omega)$, and $\Phi_{n_1,k_{y1};n_2,k_{y2}}(y,z)$ in Fourier series in terms of basis functions (5) and (6). For example, we have the following series for $\tilde{W}_{\mathbf{q}}$:

$$\tilde{W}_{\mathbf{q}}(y,z;y',z';\omega) = \sum_{g_y,g'_y}\sum_{g_z,g'_z}\left[\tilde{W}^-_{\mathbf{q},\{g_y,g_z\},\{g'_y,g'_z\}}(\omega)f^-_{g_y,g_z}(y,z)f^{-*}_{g'_y,g'_z}(y',z') + \tilde{W}^+_{\mathbf{q},\{g_y,g_z\},\{g'_y,g'_z\}}(\omega)f^+_{g_y,g_z}(y,z)f^{+*}_{g'_y,g'_z}(y',z')\right]. \tag{22}$$

The 2D Fourier transform of the Coulomb interaction (16) is expanded in Fourier series

$$V(k_x,k_y;z_1-z_2) = \sum_{g_{z_1},g_{z_2}}\left[V^-_{g_{z_1},g_{z_2}}(k_x,k_y)\frac{2}{T}\sin(g_{z_1}z_1)\sin(g_{z_2}z_2) + V^+_{g_{z_1},g_{z_2}}(k_x,k_y)\frac{\sqrt{\delta_{g_{z_1}}\delta_{g_{z_2}}}}{T}\cos(g_{z_1}z_1)\cos(g_{z_2}z_2)\right]. \tag{23}$$

Thus, integrations in Eqs. (14)–(18) turn into summations over reciprocal lattice vectors and hence the integral equation (17) turns into a matrix equation, which can be easily solved numerically. We retain five vectors g_y in expansion of wave functions (4) in the y direction (up to $|g_y|=\frac{4\pi}{a}$) and three vectors in the expansion (22): $g_y=-\frac{2\pi}{a},0,\frac{2\pi}{a}$, while 92 reciprocal lattice vectors g_z were utilized in the expansions (4), (22), and (23) in the z direction. This number of vectors is sufficient to obtain reliable results, because higher harmonics of the wave functions evaluated in our model are negligible. This fact originates from the smooth form of the 2D pseudopotential used in this work. Summation in Eq. (18) is carried out over electronic states n_1 lying below Fermi energy and over states n_2 up to energy $E_{\max}=30$ eV above Fermi level. To test the convergence of the computations with respect to the numbers of reciprocal lattice vectors and maximum energy $E_{\max}$ used, we doubled each parameter separately and the change of the calculated linewidth did not exceed 1%. So, the numerical errors of the computations are negligible compared to both the usual experimental error bar and errors, which may be introduced by the model itself.

TABLE II. Calculated linewidths $\Gamma_{e\text{-}e}$ (in meV) using both the original (O) and modified (M) 2D pseudopotentials. The meaning of the *bulk* and *surface* contributions is explained in the text. The calculated lifetime τ_{calc} (fs) $= 658/\Gamma$ (meV) contains electron-electron contribution from model M and electron-phonon contribution $\Gamma_{e\text{-}ph}$ obtained in Ref. 50. The values for Cu(111) and Ag(111) are taken from Ref. 33.

		Cu(110)		Ag(110)		Cu(111)	Ag(111)
Model	Contribution	occ	unocc	occ	unocc	occ	occ
	Surface	27	14	5.1	20		
O	Bulk	11	28	1.3	41		
	Total	38	42	6.4	61		
	Surface	11	4	1.1	6	10	1.6
M	Bulk	10	35	0.8	52	4	0.4
	Total	21	39	1.9	58	14	2
$\Gamma_{e\text{-}ph}$ $(T=0)$		9.6	4.2	6.4	2.4	8	4
τ_{calc} $(T=0)$ (fs)		22	15	79	11	30	110

III. RESULTS AND DISCUSSION

The linewidths of the surface states at the $\overline{\text{Y}}$ point of Cu(110) and Ag(110) were calculated using both the original (O) and modified (M) pseudopotential models. The results are given in Table II. The linewidth of the occupied state is determined by interband transitions to bulk states (*bulk contribution*) and intraband transitions within the occupied surface state band (*surface contribution*), while in the case of the unoccupied surface state the excited electron decays only via interband transitions. In the latter case *bulk* and *surface* contributions correspond to transitions to bulk states and to SS_{occ} bands, respectively.

As follows from the table, modification of the potential reduces significantly the contribution of intraband scattering in the occupied state, which is due to reduction of available phase space. The total linewidth of the unoccupied states remains approximately the same, while the ratio between bulk and surface contributions is changed. Later we discuss only results obtained in the model M.

Before analyzing the results of the calculations, we point out the main factors determining electron-electron scattering. The first factor is the phase space of final states for electron (hole) transitions which can be qualitatively estimated by the charge density of final states ρ^f defined as

$$\rho^f_{i\mathbf{k}_0}(y,z) = \frac{1}{(2\pi)^2}\int_{-\infty}^{+\infty} dk_x \int_{-\pi/a}^{\pi/a} dk_y \sum_n^{E_{n\mathbf{k}}\in[E_0,E_F]} |u_{nk_y}(y,z)|^2. \tag{24}$$

Figures 4(a)–4(c) demonstrate $\rho^f_{i\mathbf{k}_0}(y,z)$ as a function of z with coordinate y fixed at a value, where the initial state has a distribution maximum. The function $\rho^f_{\text{unocc}}(y=0,z)$ for the unoccupied surface states is determined only by bulk electronic states, because the charge density of the occupied surface states at $y=0$ is equal to zero. The function $\rho^f_{\text{occ}}(y=a/2,z)$ for occupied surface states includes both bulk states (interband) contribution and SS_{occ}-band (intraband) contribution. The latter contribution is smaller by a factor of two than the former one at the probability maximum point of the occupied surface state located at $z \approx -0.1a_s$ relative to the outermost atomic layer.

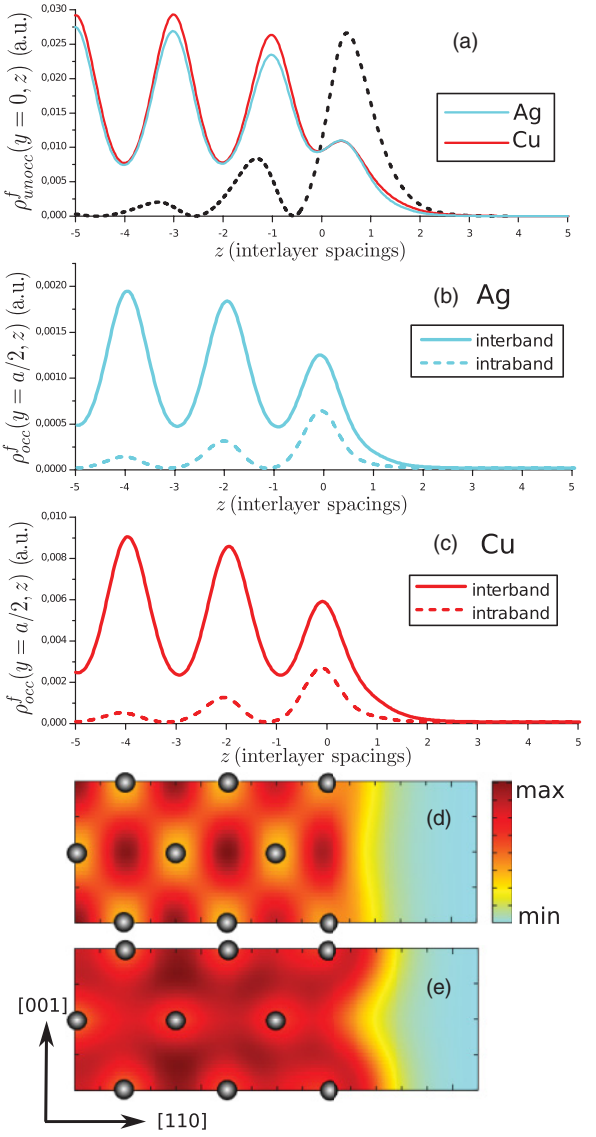

FIG. 4. (Color online) Charge density of final states $\rho^f_{\text{unocc}}(y=0,z)$ for decay of the unoccupied states on Cu and Ag (a); $\rho^f_{\text{occ}}(y=a/2,z)$ for the occupied states on Ag (b) and Cu (c), calculated within model M. ρ^f is divided into interband (solid lines) and intraband (dashed lines) contributions for the occupied states. The black dotted line in (a) shows the localization of the unoccupied surface state in arbitrary units normalized so as to be plotted on the same scale as ρ^f_{unocc}. The localization of the occupied states coincides with the intraband contribution to ρ^f_{occ} indicated by dashed lines in (b) and (c). The origin $z=0$ corresponds to the outermost atomic layer. Distribution of ρ^f_{unocc} for Ag(110) in the $(1\bar{1}0)$ plane averaged over the $[1\bar{1}0]$ direction, calculated within model M (d) and the DFT with HGH pseudopotential (e). Gray balls denote the positions of atomic chains in the $[1\bar{1}0]$ direction.

Figure 4(d) shows the distribution of the charge density of final states $\rho^f_{\text{unocc}}(y,z)$ for the unoccupied surface state on Ag(110) in the $(1\bar{1}0)$ plane. The corresponding distribution for SS_{occ} is qualitatively similar to that for SS_{unocc} and is not shown here. One can see that the maxima of ρ^f_{unocc} are

located between the atomic chains, while the minima lie at the positions of the atomic chains in the $[1\bar{1}0]$ direction. Since our model does not describe the effects of d electrons on the decay of excitations in the surface states, we compare the model M pseudopotential charge densities with those obtained from first-principle calculations, which use pseudopotentials with no d electrons included into the valence shells. Figure 4(e) shows the DFT-derived function ρ^f_{unocc} for Ag(110), calculated by means of the ABINIT[58,59] code with the norm-conserving Hartwigsen-Goedecker-Hutter (HGH) pseudopotential,[60] which considers only the $5s$ electron as the valence one, while other electrons are included into the core. As can be seen in Figs. 4(d) and 4(e) the functions ρ^f_{unocc} calculated from model M and the DFT are qualitatively similar.

The second factor responsible for the decay is the imaginary part of the screened interaction, $\text{Im}\tilde{W}$, which depends on the wave vector $\mathbf{q}$ and frequency ω. Figure 5 plots local ($z = z'$) and nonlocal ($z \neq z'$) functions $\text{Im}\tilde{W}_{\mathbf{q}}(y,z;y',z')$ for different values of $\mathbf{q}$ and ω. Three general trends can be found in Fig. 5: (1) the higher the frequency ω, the larger is the magnitude of $|\text{Im}\tilde{W}_{\mathbf{q}}(\omega)|$; (2) small wave vectors (in the $x-y$ plane) cause long-range interaction in the z direction with large magnitude; (3) $|\text{Im}\tilde{W}_{\mathbf{q}}(\omega)|$ is larger in silver than in copper for the same values of $\mathbf{q}$ and ω. The first trend comes from the properties of linear response function χ, while the second one follows directly from the form of the bare Coulomb potential (16). The last feature is explained by lower electronic density in silver, which causes weaker screening of the interaction in Ag and thus stronger scattering.

Now we return to the linewidth results. As can be seen from Table II, excitations in the unoccupied states decay mostly via transitions into bulk states. The contribution from transitions between two surface states is small because these states are spatially separated, and the phase space volume, where the lower surface state lies in the gap above E_F, is very small. The linewidth of SS_{unocc} on Ag is 1.5 times larger than the linewidth of SS_{unocc} on Cu. The reasons of this result can be understood from the following. As one can see in Fig. 4(a), ρ^f for SS_{unocc} on Ag is slightly smaller than that on Cu because of a small difference in energies of these states. Thus, the difference in the linewidth may only be caused by greater magnitude of $\text{Im}\tilde{W}_{\mathbf{q},\omega}$. Comparison of Figs. 5(a) and 5(b) demonstrates that $|\text{Im}\tilde{W}_{\mathbf{q},\omega}|$ in Ag is about 1.5 times larger than in Cu for the same values of $\mathbf{q}$ and ω. Indeed, this fact is responsible for the difference of the decay rates of unoccupied surface states in Cu and Ag.

Approximately equal contributions have been obtained for inter- and intraband scattering channels of the occupied states on both Cu(110) and Ag(110). In this case the two factors compensate each other. On the one hand, the contribution of bulk states to the density of final states ρ^f_{occ} is higher than the corresponding contribution of the occupied surface state. Figures 4(b) and 4(c) demonstrate that ρ^f_{occ} at $y = a/2$ (where the occupied surface state is mainly localized) has a larger contribution from bulk states than from the surface state itself. On the other hand the intraband scattering occurs with smaller change of wave vector, and that results in a greater magnitude of $\text{Im}\tilde{W}$, as one can see in Fig. 5(c).

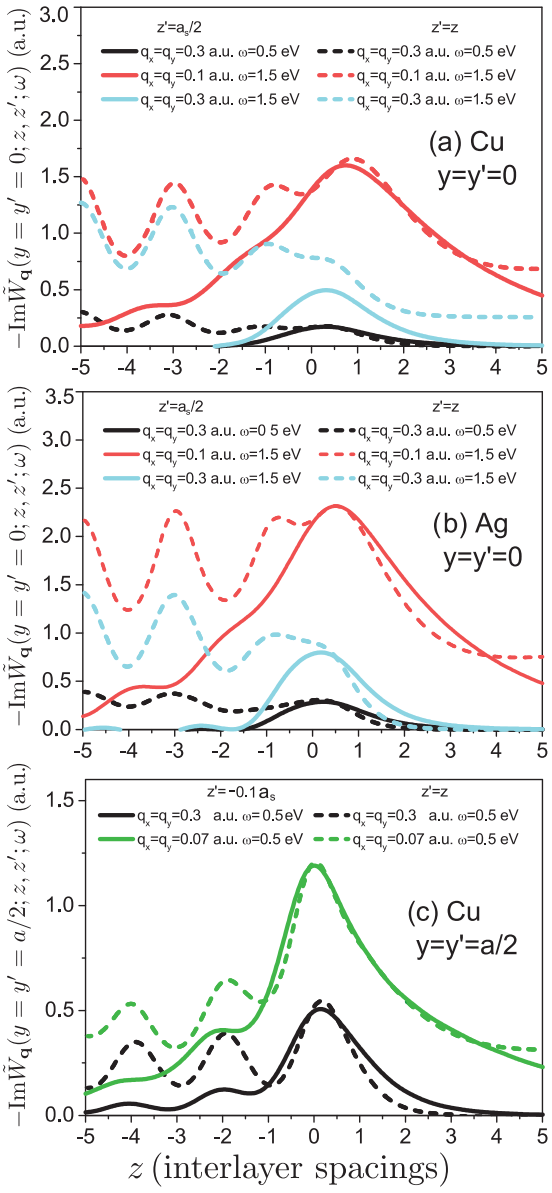

FIG. 5. (Color online) $-\text{Im}\tilde{W}_{\mathbf{q}\omega}(y,z;y',z')$ as a function of z with $y = y' = 0$ (a),(b) and $y = y' = a/2$ (c) for different values of $\mathbf{q}$ and ω. The origin $z = 0$ corresponds to the outermost atomic layer. Dashed lines denote local ($z = z'$) interaction; solid lines show nonlocal interaction, z' being fixed at $z' = a_s/2$ (a),(b) and $z' = -0.1a_s$ (c).

The energy of the occupied surface state at the $\overline{\text{Y}}$ point on the (110) surfaces of Cu and Ag relative to the Fermi level and the gap edge are similar to those on the respective (111) surfaces, so it is reasonable to compare them. Intraband contributions calculated[33] for the surface states on Cu(111) and Ag(111) are approximately equal to that of Cu(110) and Ag(110), respectively. However, sufficiently larger interband contributions were obtained on the (110) surfaces. The reason is twofold. First, the occupied state on (110) penetrates deeper into the crystal than on (111) that results in larger overlap with bulk electronic states. Second, the bottom edge of the gap on (110) has smaller effective mass than that on (111). This yields smaller wave vectors for interband transitions and

consequently greater magnitude of the imaginary part of the screened interaction $\mathrm{Im}\tilde{W}$.

The calculated linewidth of the occupied state on Cu(110) can be compared with the photoemission value $\Gamma_{\mathrm{exp}} = 48 \pm 6$ meV at $T = 140$ K.[39] Electron-phonon contribution to the linewidth for this temperature, accordingly to both the same experiment and our previous calculations,[48] is equal to 17 meV, and thus $\Gamma_{\mathrm{calc}} = \Gamma_{e-ph} + \Gamma_{e-e} = 38$ meV. As far as our calculations give the lower limit for the linewidth, whereas the experiment gives the upper one, this may be considered as a good agreement. The difference of 10 ± 6 meV may be attributed to electron-defect scattering. It should be noted that the lifetime of the occupied surface state on Cu(110) has also been obtained from *ab initio* calculations,[38] $\tau = 82$ fs, that corresponds to a linewidth $\Gamma = \hbar/\tau = 8$ meV. This result differs significantly from our value because an approximation made in Ref. 38 assumed the self-energy operator to be equal to that in the bulk crystal. Consequently, the intraband scattering and the change of screening in the surface region were not accounted for. We find that the value of Ref. 38 is just 3 meV smaller than our result for interband contribution. This difference may be attributed to neglecting the role of the surface in screening of the Coulomb interaction, because, as one can see from Fig. 5(c), $|\mathrm{Im}\tilde{W}(y = y' = a/2)|$ is slightly larger in the surface region than in the bulk.

IV. CONCLUSIONS

We have developed the method of calculating many-body electron-electron scattering contribution to the linewidth of electrons and holes in surface states on the (110) surfaces of fcc metals, based on recently elaborated 2D pseudopotential model. We have modified this model to reproduce correctly the dispersion of surface states and bulk gap edges. On the basis of this method we have performed a comparative study of many-body electron-electron scattering for electrons and holes in the surface states on Cu(110) and Ag(110). We find that the excited electrons in the unoccupied states have larger linewidths than holes in the occupied states because of their higher binding energy and, respectively, bigger phase space for electron transitions. The linewidth of the unoccupied surface state on Ag(110) is larger than on Cu(110) because of weaker screening in Ag. Another feature of the unoccupied state is that the excited electrons decay mostly via transitions into bulk states. The contribution of electron-electron scattering into the lower surface band is small due to little overlap of the surface states and small phase space for electron transitions to this band. Equal contributions are obtained for inter- and intraband scattering of the excited holes. We have also shown that the excited holes on Cu(110) decay faster than on Cu(111) due to a bigger interband contribution. The linewidth of a hole on Ag(110) is small because it lies close to Fermi level, and it is practically equal to that of the $\overline{\Gamma}$ surface state on Ag(111). Our value $\Gamma_{e\text{-}e}$ in combination with the calculated earlier electron-phonon contribution $\Gamma_{e\text{-}ph}$ gives the linewidth of the occupied surface state on Cu(110) in a good agreement with available photoemission data. The developed method together with the previously proposed method for calculating electron-phonon scattering makes it possible to comprehensively describe the quasiparticle excitations on (110) noble metal surfaces.

ACKNOWLEDGMENTS

We acknowledge the partial support from the University of the Basque Country (Grant No. IT-366-07), the Departamento de Educación del Gobierno Vasco, Ministerio de Ciencia e Inovación (Grant No. FIS2010-19609-C02-01), and the Russian Ministry of education and science (Contract No. P2366). Calculations were performed on the SKIF-Cyberia supercomputer of Tomsk State University.

[1] E. Knoesel, A. Hotzel, and M. Wolf, Phys. Rev. B **57**, 12812 (1998).
[2] M. Aeschlimann, M. Bauer, S. Pawlik, W. Weber, R. Burgermeister, D. Oberli, and H. C. Siegmann, Phys. Rev. Lett. **79**, 5158 (1997).
[3] H. Petek, H. Nagano, and S. Ogawa, Phys. Rev. Lett. **83**, 832 (1999).
[4] I. Campillo, V. M. Silkin, J. M. Pitarke, E. V. Chulkov, A. Rubio, and P. M. Echenique, Phys. Rev. B **61**, 13484 (2000)
[5] V. P. Zhukov, F. Aryasetiawan, E. V. Chulkov, and P. M. Echenique, Phys. Rev. B **65**, 115116 (2002).
[6] V. P. Zhukov, E. V. Chulkov, and P. M. Echenique, Phys. Rev. Lett. **93**, 096401 (2004).
[7] U. Höfer, I. L. Shumay, Ch. Reuss, U. Thomann, W. Wallauer, and Th. Fauster, Science **277**, 1480 (1997).
[8] M. Wolf, E. Knoesel, and T. Hertel, Phys. Rev. B **54**, 5295(R) (1996).
[9] E. V. Chulkov, V. M. Silkin, and M. Machado, Surf. Sci. **482–485**, 693 (2001).
[10] S. Link, H. A. Dürr, G. Bihlmayer, S. Blügel, W. Eberhardt, E. V. Chulkov, V. M. Silkin, and P. M. Echenique, Phys. Rev. B **63**, 115420 (2001).
[11] H. Petek and S. Ogawa, Annu. Rev. Phys. Chem. **53**, 507 (2002).
[12] A. Schäfer, I. L. Shumay, M. Wiets, M. Weinelt, Th. Fauster, E. V. Chulkov, V. M. Silkin, and P. M. Echenique, Phys. Rev. B **61**, 13159 (2000).
[13] M. Weinelt, J. Phys. Condens. Matter **14**, R1099 (2002).
[14] U. Bovensiepen, Prog. Surf. Sci. **78**, 87 (2005).
[15] A. B. Schmidt, M. Pickel, M. Donath, P. Buczek, A. Ernst, V. P. Zhukov, P. M. Echenique, L. M. Sandratskii, E. V. Chulkov, and M. Weinelt, Phys. Rev. Lett. **105**, 197401 (2010).
[16] E. V. Chulkov, J. Kliewer, R. Berndt, V. M. Silkin, B. Hellsing, S. Crampin, and P. M. Echenique, Phys. Rev. B **68**, 195422 (2003).
[17] C. Corriol, V. M. Silkin, D. Sánchez-Portal, A. Arnau, E. V. Chulkov, P. M. Echenique, T. von Hofe, J. Kliewer, J. Kröger, and R. Berndt, Phys. Rev. Lett. **95**, 176802 (2005).
[18] C. H. Schwalb, S. Sachs, M. Marks, A. Schöll, F. Reinert, E. Umbach, and U. Höfer, Phys. Rev. Lett. **101**, 146801 (2008).
[19] P. S. Kirchmann, L. Rettig, X. Zubizarreta, V. M. Silkin, E. V. Chulkov, and U. Bovensiepen, Nat. Phys. **6**, 782 (2010); R. Dez Muiño, D. Sánchez-Portal, V. M. Silkin, E. V. Chulkov, and P. M. Echenique, Proc. Natl. Acad. Sci. USA **108**, 971 (2011).

[20] S. Mathias, A. Ruffing, F. Deicke, M. Wiesenmayer, M. Aeschlimann, and M. Bauer, Phys. Rev. B **81**, 155429 (2010).
[21] M. Bauer, S. Pawlik, and M. Aeschlimann, Phys. Rev. B **60**, 5016 (1999).
[22] S. Ogawa, H. Nagano, and H. Petek, Phys. Rev. Lett. **82**, 1931 (1999).
[23] A. G. Borisov, J. P. Gauyacq, E. V. Chulkov, V. M. Silkin, and P. M. Echenique, Phys. Rev. B **65**, 235434 (2002).
[24] A. G. Borisov, V. Sametoglu, A. Winkelmann, A. Kubo, N. Pontius, J. Zhao, V. M. Silkin, J. P. Gauyacq, E. V. Chulkov, P. M. Echenique, and H. Petek, Phys. Rev. Lett. **101**, 266801 (2008).
[25] S. Achilli, M. I. Trioni, E. V. Chulkov, P. M. Echenique, V. Sametoglu, N. Pontius, A. Winkelmann, A. Kubo, J. Zhao, and H. Petek, Phys. Rev. B **80**, 245419 (2009).
[26] A. G. Borisov, T. Hakala, M. J. Puska, V. M. Silkin, N. Zabala, E. V. Chulkov, and P. M. Echenique, Phys. Rev. B **76**, 121402(R) (2007).
[27] C. Tournier-Colletta, B. Kierren, Y. Fagot-Revurat, and D. Malterre, Phys. Rev. Lett. **104**, 016802 (2010).
[28] M. Bonn, S. Funk, Ch. Hess, D. N. Denzler, C. Stampfl, M. Scheffler, M. Wolf, and G. Ertl, Science **285**, 1042 (1999).
[29] H. Nienhaus, Surf. Sci. Rep. **45**, 1 (2002).
[30] C. D. Lindstrom and X.-Y. Zhu, Chem. Rev. **106**, 4281 (2006).
[31] N. Memmel and E. Bertel, Phys. Rev. Lett. **75**, 485 (1995).
[32] P. M. Echenique, R. Berndt, E. V. Chulkov, Th. Fauster, A. Goldmann, and U. Höfer, Surf. Sci. Rep. **52**, 219 (2004).
[33] E. V. Chulkov, A. G. Borisov, J. P. Gauyacq, D. Sanchez-Portal, V. M. Silkin, V. P. Zhukov, and P. M. Echenique, Chem. Rev. **106**, 4160 (2006).
[34] A. Eiguren, B. Hellsing, E. V. Chulkov, and P. M. Echenique, Phys. Rev. B **67**, 235423 (2003).
[35] Ph. Hofmann, I. Yu. Sklyadneva, E. D. L. Rienks, and E. V. Chulkov, New J. Phys. **11**, 125005 (2009).
[36] M. Fuglsang Jensen, T. K. Kim, S. Bengió, I. Y. Sklyadneva, A. Leonardo, S. V. Eremeev, E. V. Chulkov, and Ph. Hofmann, Phys. Rev. B **75**, 153404 (2007).
[37] S. V. Eremeev and E. V. Chulkov, Phys. Solid State **51**, 854 (2009).
[38] R. Keiling, W.-D. Schöne, and W. Ekardt, Chem. Phys. Lett. **354**, 376 (2002).
[39] P. Straube, F. Pforte, T. Michalke, K. Berge, A. Gerlach, and A. Goldmann, Phys. Rev. B **61**, 14072 (2000).
[40] A. Mugarza, A. Mascaraque, V. Repain, S. Rousset, K. N. Altmann, F. J. Himpsel, Yu. M. Koroteev, E. V. Chulkov, F. J. García de Abajo, and J. E. Ortega, Phys. Rev. B **66**, 245419 (2002).
[41] S. M. Dounce, M. Yang, and H.-L. Dai, Phys. Rev. B **67**, 205410 (2003).
[42] G. A. Somorjai, in *Elementary Reaction Step in Heterogeneous Catalysis*, edited by R. W. Joyner and R. A. Van Santen (Kluwer, Dordrecht, 1993), p. 3.
[43] E. V. Chulkov, V. M. Silkin, and P. M. Echenique, Surf. Sci. **391**, L1217 (1997); **437**, 330 (1999).
[44] A. Gerlach, G. Meister, R. Matzdorf, and A. Goldmann, Surf. Sci. **443**, 221 (1999).
[45] O. Zeybek, A. M. Davarpanah, and S. D. Barrett, Surf. Sci. **600**, 5176 (2006).
[46] A. Goldmann, V. Dose, and G. Borstel, Phys. Rev. B **32**, 1971 (1985).
[47] S. S. Tsirkin, S. V. Eremeev, and E. V. Chulkov, Phys. Solid State **52**, 188 (2010).
[48] S. S. Tsirkin, S. V. Eremeev, and E. V. Chulkov, Surf. Sci. **604**, 804 (2010).
[49] S. V. Eremeev, S. S. Tsirkin, and E. V. Chulkov, JETP **110**, 788 (2010).
[50] S. V. Eremeev, S. S. Tsirkin, and E. V. Chulkov, Phys. Rev. B **82**, 035424 (2010).
[51] G. Kresse and J. Hafner, Phys. Rev. B **48**, 13115 (1993).
[52] G. Kresse and J. Furthmüller, Comput. Mater. Sci. **6**, 15 (1996).
[53] P. E. Blöchl, Phys. Rev. B **50**, 17953 (1994).
[54] G. Kresse and D. Joubert, Phys. Rev. B **59**, 1758 (1999).
[55] J. P. Perdew, K. Burke, and M. Ernzerhof, Phys. Rev. Lett. **77**, 3865 (1996).
[56] W. Jacob, V. Dose, U. Kolac, Th. Fauster, and A. Goldmann, Z. Phys. B **63**, 459 (1986).
[57] L. Hedin, Phys. Rev. **139**, A796 (1965).
[58] X. Gonze, B. Amadon, P.-M. Anglade, J.-M. Beuken, F. Bottin, P. Boulanger, F. Bruneval, D. Caliste, R. Caracas, M. Cote, T. Deutsch, L. Genovese, Ph. Ghosez, M. Giantomassi, S. Goedecker, D. R. Hamann, P. Hermet, F. Jollet, G. Jomard, S. Leroux, M. Mancini, S. Mazevet, M. J. T. Oliveira, G. Onida, Y. Pouillon, T. Rangel, G.-M. Rignanese, D. Sangalli, R. Shaltaf, M. Torrent, M. J. Verstraete, G. Zerah, and J. W. Zwanziger, Comput. Phys. Commun. **180**, 2582 (2009).
[59] X. Gonze, G.-M. Rignanese, M. Verstraete, J.-M. Beuken, Y. Pouillon, R. Caracas, F. Jollet, M. Torrent, G. Zerah, M. Mikami, Ph. Ghosez, M. Veithen, J.-Y. Raty, V. Olevano, F. Bruneval, L. Reining, R. Godby, G. Onida, D. R. Hamann, and D. C. Allan, Z. Kristallogr. **220**, 558 (2005).
[60] C. Hartwigsen, S. Goedecker, and J. Hutter, Phys. Rev. B **58**, 3641 (1998).